DEFORMATION OF SHEARED MARGINAL GRANITES AND THE FORCEFUL EMPLACEMENT OF THE TUNGSTONIA PLUTON, KERN MOUNTAINS, NEVADA

An Undergraduate Research Scholars Thesis

by

TRAVIS FLINT HAGER

Submitted to the Undergraduate Research Scholars program
Texas A&M University
in partial fulfillment of the requirements for the designation as an

UNDERGRADUATE RESEARCH SCHOLAR

Approved by
Research Advisor: Dr. Andreas Kronenberg

May 2016

Major: Geology

TABLE OF CONTENTS

Page

ABSTRACT

Deformation of Sheared Marginal Granites and the Forceful Emplacement of the Tungstonia Pluton, Kern Mountain, Nevada

Travis F. Hager
Department of Geology and Geophysics
Texas A&M University

Research Advisor: Dr. Andreas Kronenberg
Department of Geology and Geophysics

Marginal granites of the Tungstonia Pluton of the Kern Mountains, Eastern Nevada, are foliated with poles to foliation that are nearly parallel to those of foliations developed in surrounding dolostones. Thus, the dolostones and marginal granites appear to have deformed during forceful magma emplacement. Previous studies of the foliated dolostones indicate that penetrative strains in the surrounding country rock were accommodated by high temperature creep within a narrow (<400m) zone that corresponds to a narrow contact metamorphic aureole. The foliated granites within the Tungstonia Pluton are interpreted to be the first-crystallized plutonic rocks, which were then subjected to stresses of the intrusion event soon after crystallization.

Microstructures of the foliated granites are under investigation by optical microscopy, in order to determine their intragranular strains and the mechanisms by which these rocks deformed. Quartz grains are highly sheared with locally large aspect ratios and micas show alignment. Quartz grains also show evidence of dynamic recrystallization. In contrast, most feldspar grains appear undeformed, and only occasional feldspar grains show deformation microstructures. Quartz grain shapes will be used to estimate their intragranular strains and alignments of quartz c-axes (and mica grains) will be used to evaluate strain patterns and conditions of deformation. These

rocks represent a continuum of solid-state deformation surrounding the central intruding melt of the pluton, with shear in dolomites throughout the history of magma injection, and later shear of cooled and crystallized granite as the melt body was reduced in size but was still buoyant.

ACKNOWLEDGMENTS

I would like to thank and express my sincerest gratitude to my academic research advisor, Dr. Andreas Kronenberg, for offering not only his expertise and guidance, but his faith that I would fulfill his expectations by suggesting this research project to me. I would like to further acknowledge the considerable time commitment it took on his part to offer me mentorship and editorial contributions.

I would like to acknowledge and thank both Kyle Goodson and William Shea; whose work and efforts have laid the groundwork that made this research project possible. I sincerely hope that they are proud of the results their contributions have led to.

Finally, I would like to take this opportunity to further extend my expression of gratitude to all the professors in the Texas A&M Department of Geology and Geophysics whose personal drive and enthusiasm for their work extends beyond their own studies and into the classroom where their passion has inspired myself and will continue inspire the next generation of geoscientists.

FIGURE LIST

Page

TABLE LIST

Page

CHAPTER I

INTRODUCTION

The nature and mechanics by which volumetrically large igneous bodies are transported and subsequently emplaced in Earth's subsurface is a subject of considerable interest and scrutiny in field of structural geology. This interest arises from how different emplacement models solve for what is classically described as the 'room problem'; or how a magmatic body displaces an equivalent volume of country rock during its ascent (Bowen, 1948). This equivalence is fundamentally derived from the principle of the conservation of mass wherein matter can never be created or destroyed but is rather rearranged and transported in space. With respect to this fundamental principle and perspective framed in terms of the Tungstonia pluton, this investigation hopes to better understand the role of magmatic bodies in the transportation of matter in the subsurface.

In the low pressure regions of the upper crust with smaller volumes of magma that are dominated by brittle deformation processes, mechanisms that create formations such as dikes and sills, magma filling in openings in the form of either vertical or horizontal fractures respectively, or subsequent laccoliths, where ample magma pressures cause dikes and sills to inflate and leads the country rock to accommodate this inflation by uplifting the overbearing country rock, are well understood and documented (Hunt et al, 1953; Pollard and Johnson,1973; Gilbert, 1977; Shaw, 1980; Holder, 1981; Morgan et al., 1998; Gerbi et al., 2004). Furthermore, these processes typically generate low strains with little deformation recorded in the surrounding country rock (Clemens, 1998). Conversely, large volumes of magma must displace equally large volumes of

country rock, and significant strains are expected to be present in the contact metamorphic aureole and the intruding body itself (Marsh, 1982, Miller & Patterson, 1999, Gerbi et al., 2004, Zak & Patterson, 2006). At greater depths and consequentially greater pressures and temperatures, brittle rock mechanics give way to crystal-plastic, ductile ones leaving intruding igneous bodies to progress through greater vertical distances without the luxury of being able to inject into fractures and uplift overburden. This results in the ascending magmatic body having to either forcefully penetrate and deform the superimposed strata in order to emplace at shallow crustal depths or have that overburden tectonically removed to allow the magma to ascend into a freshly generated chamber without the need for significant magma injection and penetration into the country rock. Models exist for both of these contrasting emplacement mechanisms, however large volume plutonic displacements are typically less understood and more difficult to constrain and model relative to their low pressure, low volume counterparts. As a result, the field remains divided on how to best solve the ‘room problem’ where large volumes of magma are involved.

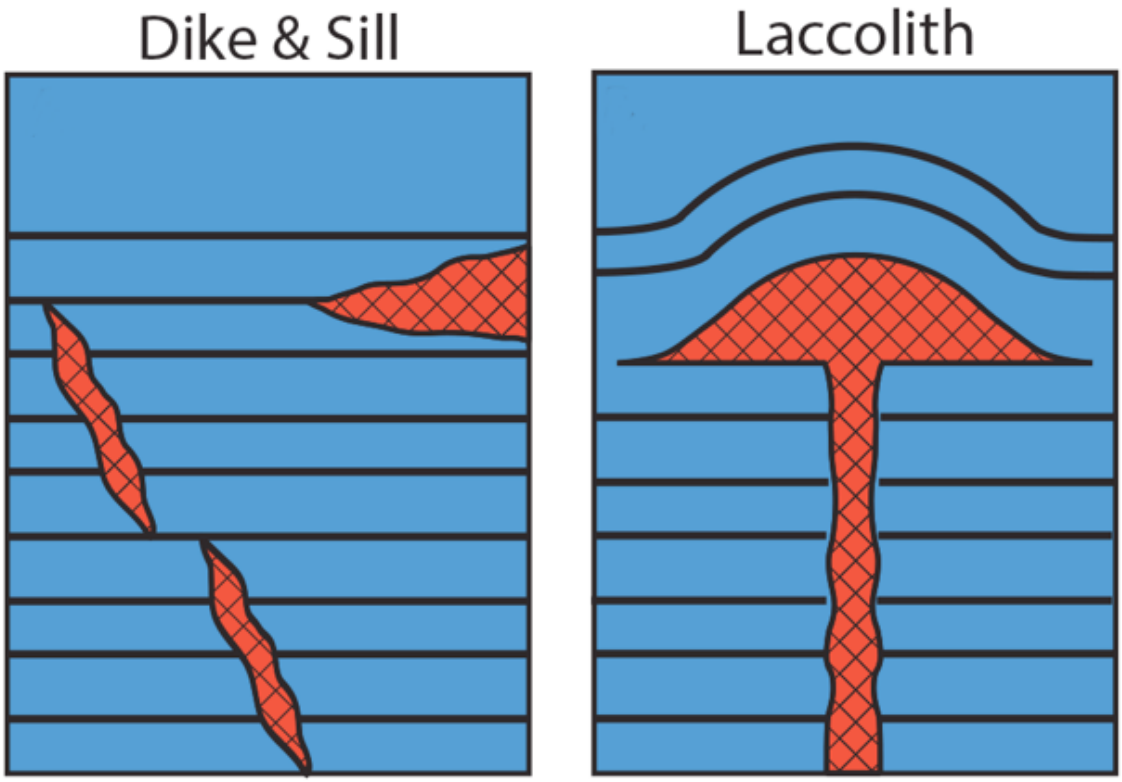

Figure 1. General emplacement model for dikes, sills, and laccoliths of low pressure, brittle regions of the upper crust after Shea et al., 1988 and Goodson, 2014

Contrasting models of plutonic emplacement include tectonic displacement, stoping, inflation, and diapirism. In extensional tectonic settings or other areas with considerable faults, folds, and other such deformation, igneous plutons have been shown to ‘passively’ emplace or translate upward by means of tectonic accommodation where there is considerable lateral displacement of country rocks (Tikoff and Teyssier, 1992, Tikoff et al., 1999). While this mechanism describes pluton emplacement for particular geologic settings, not all plutons intrude into these particular regions. Consequently, various geologic occurrences must be resolved by means of forceful emplacement methods where magma must penetrate and deform the country rock to solve the

‘room problem’ of its own vocation without predominant tectonic accommodation (Marsh, 1982; Tikoff et al., 1999).

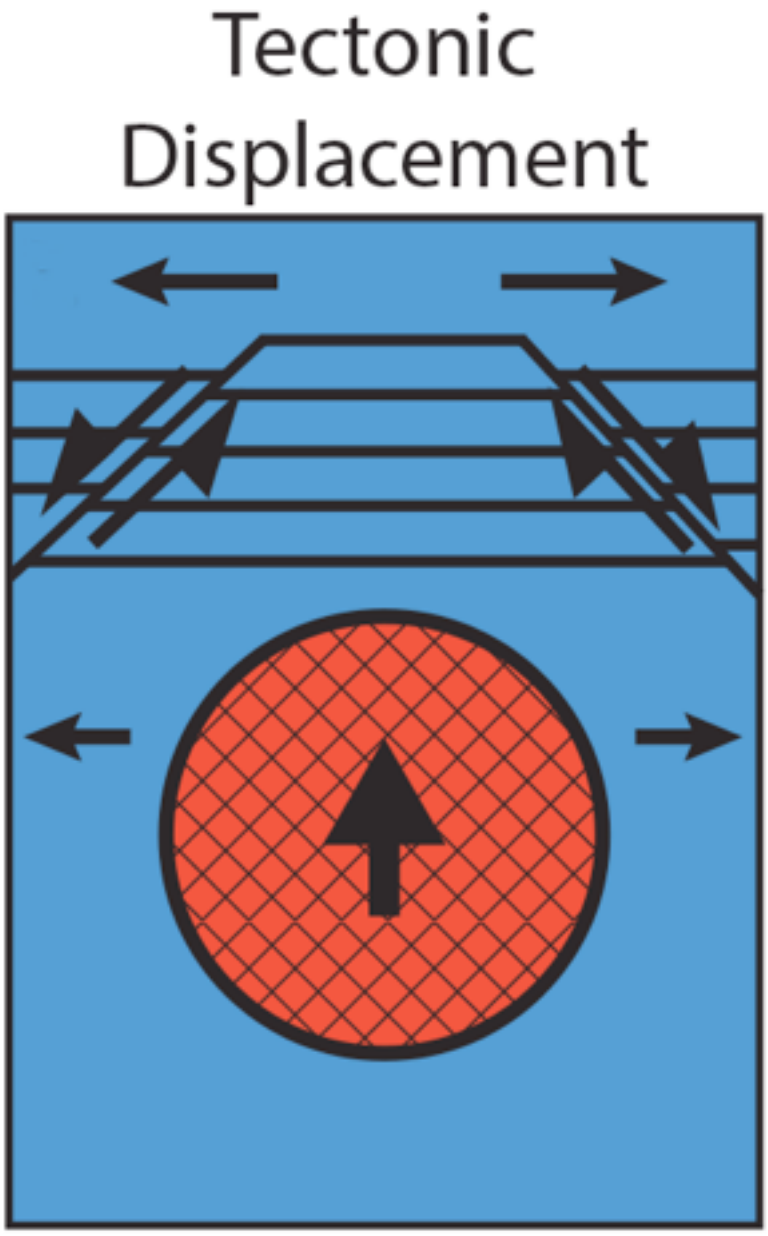

Figure 2. General passive emplacement model for tectonic accommodation after Shea et al., 1988 and Goodson, 2014. Lateral arrows indicate direction of crustal displacement while the arrow inside the pluton model indicates the ascent direction

Stoping is a forceful emplacement process by which large chunks of surrounding country rock break off and are absorbed into the rising igneous body (Daly, 1903). The heat and pressure of the igneous intrusion contrasts that of the cold country rock above it and cause fractures to form. Once these fractures fail, overbearing blocks of country rock fall into and through a rising magma chamber. This may be expressed geologically in a pluton with discordant contacts surrounding the main body of the pluton with profound offshooting dikes or fractures in the surrounding country rock (Shea et al., 1988). Another feature characteristic of a stoping event, Xenoliths, compositionally unique fragments of rock within a larger igneous body, are integrated within the rising magma chamber as country rock falls into and is then enveloped within the crystallizing body. However, the addition of these much colder and chemically diverse host rocks to the intrusion can start a crystallization event as the rocks lower the temperature of the magma body or geochemically alter its composition. Consequently, this mechanism has been determined to be thermally ineffective for larger granitic bodies at a significant scale (Marsh, 1982).

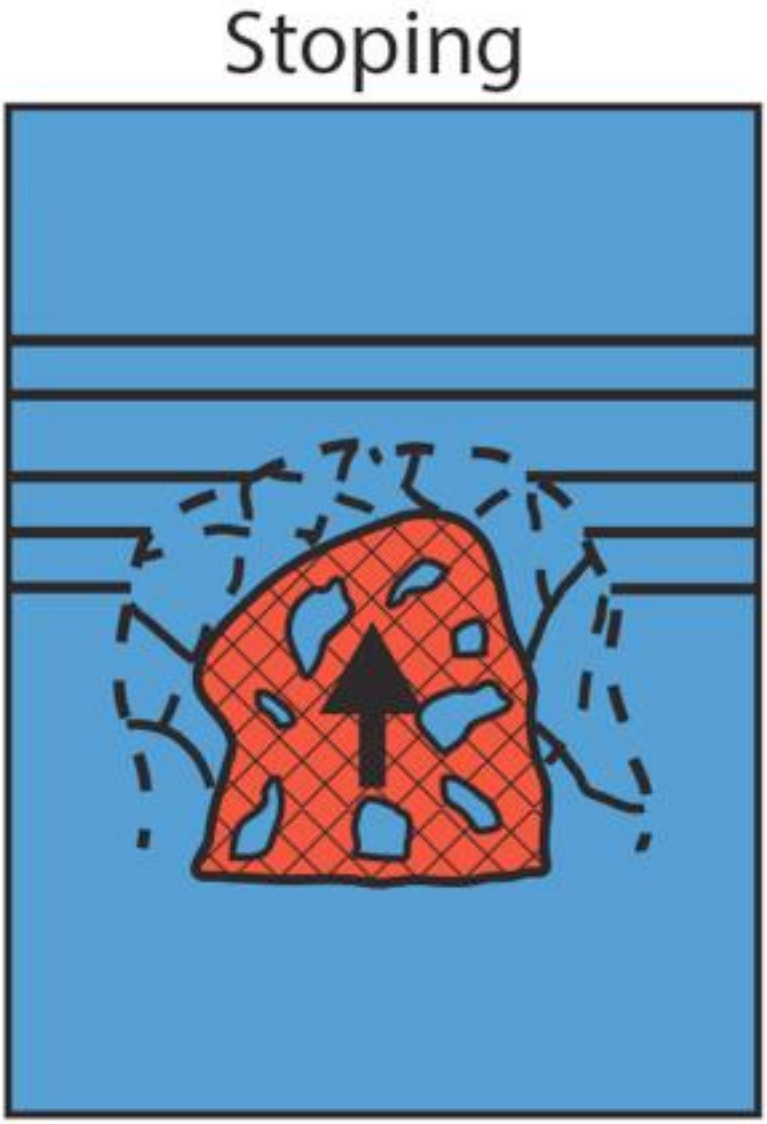

Figure 3. General forceful emplacement model for stoping after Shea et al., 1988 and Goodson, 2014. Blue fragments inside rising magma body indicate xenolith incorporation into ascending magma body

Similar to the strains expected of expanding laccoliths, inflation describes a method of forceful emplacement where the buoyant forces of the rising granitic pluton expands and pushes against the lithostatic pressure generated by the enveloping country rock (Clifford, 1972; Holder, 1979).

This emplacement model geologically expresses itself with concordant contacts with foliations that are sub-parallel to the contact. Consequently, the strain ellipsoid generated in this field of intrusion is one of coaxial pure strain wherein shortening is expected to parallel the contact while the other two major finite strain axes equivalently extend perpendicular to the contact (Shea et al., 1988)

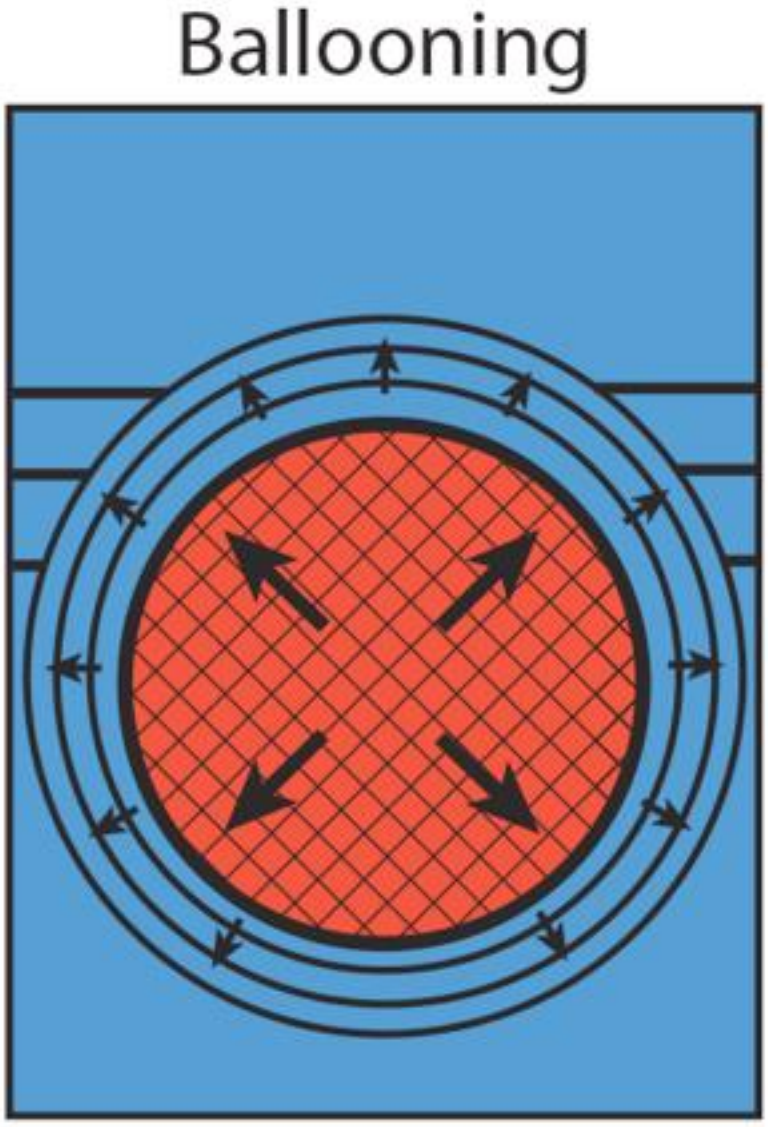

Figure 4. General forceful emplacement model for inflation or ballooning mechanism after Shea et al., 1988 and Goodson, 2014

Diapirism is another subsect of forceful emplacement where the hot spherical magma body lowers the viscosity of country rock and deforms in a thin margin along its edges during its ascent due to thermal weakening. By this mechanism, non-linear viscosities of host rock localize flow to a thin channel down the sides of the rising body while minimizing heat loss, and simple shear and high temperatures deforms the country rocks and the margins of the granite (Miller & Paterson, 1999; Vilgneresse & Clemens, 2000; Polyansky et al., 2009; Polyansky et al., 2010; Paterson et al., 2011; Schmeling, 1988). If it solidifies, the magmatic diapir may still rise several kilometers in a solid state if its density contrasts with that of the surrounding country rock due to buoyant forces (Vilgneresse & Clemens, 2000). This style of forceful emplacement generates high strain rates along its margins and low strain rates at its core due to the laminar channel flow that displaces the country rock allowing the diapir to emplace (Weinberg and Podladchikov, 1995; Schmeling, 1988). Once again, concordant contacts and foliations sub-parallel to those contacts are expected at the margins contrasting the country rock and the granitic body (Shea et al., 1988). However, the rising diapir generates strain ellipsoids in all three characteristic fields at different parts of the diapir's margins. Compressional pure strain is expected in the margin in contact with the directly overlain country rock, and simple shear strain is expected along the side margin where the country rock/ granite pluton contact is found on the exposed surface (Schmeling, 1988). Furhtermore, extensional strain is expected below the rising diapir (Schmeling, 1988).

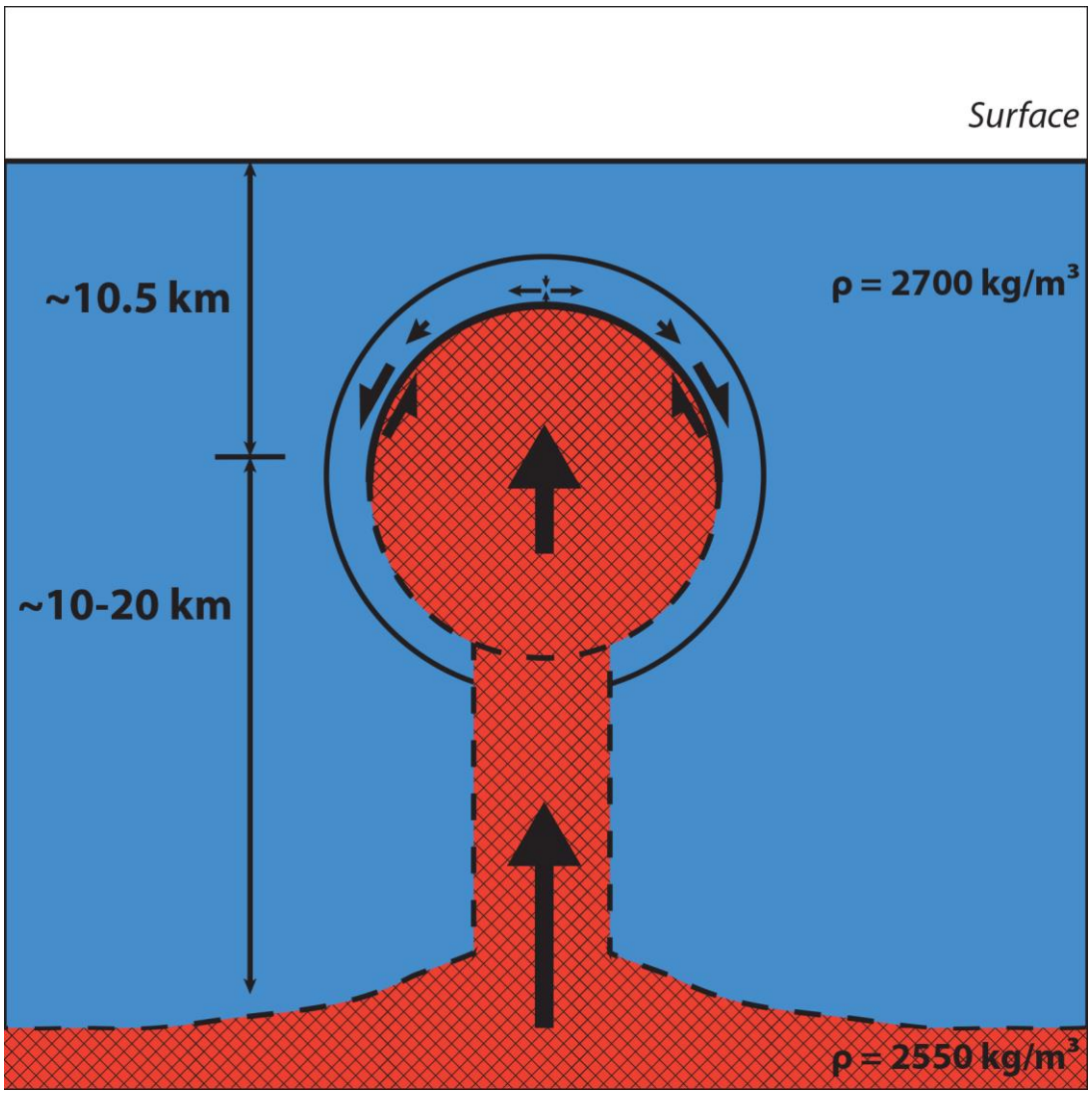

Figure 5. General emplacement model for the diapiric ascent of the Tungstonia Granite. Pure shear indicated by arrows directly above the body's ascent direction (indicated in the sphereical pluton body and column below) after Shea et al., 1988 and Goodson, 2014. Simple shear indicated by arrows along the sides of the model. Densities and relative speculated depth given as well

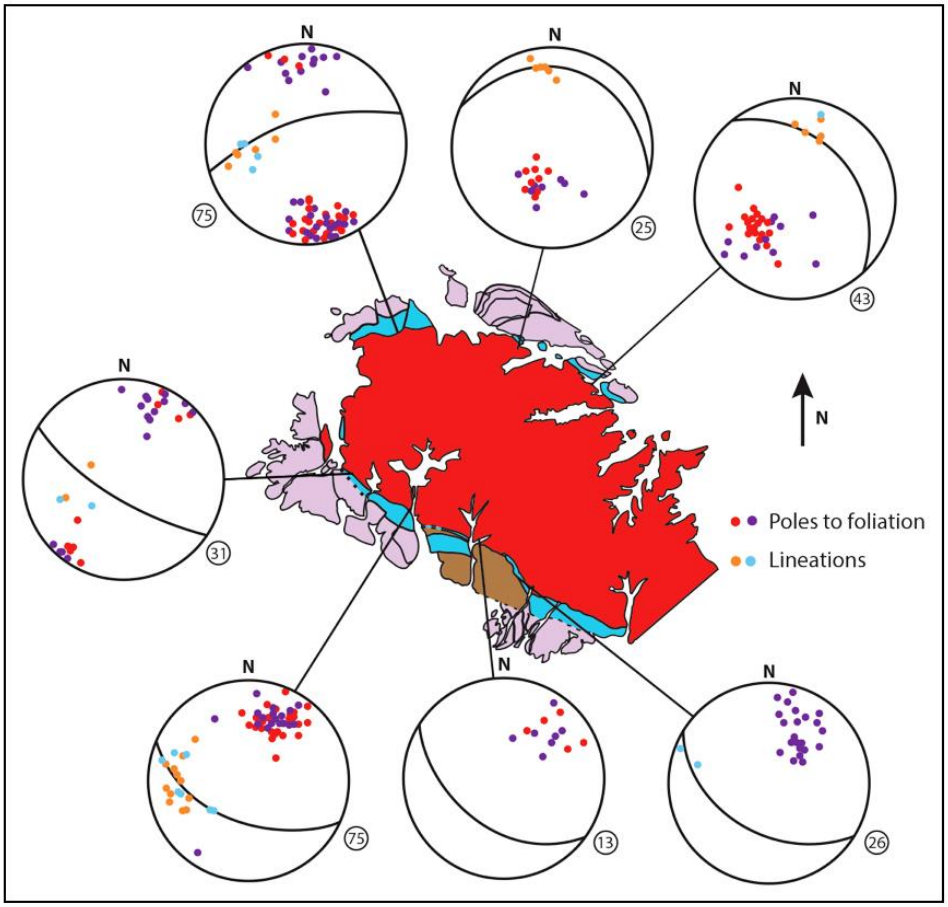

Figure 6. Poles to foliation and lineations from the Kern Mountain granites and dolostones. Foliations dip away from the pluton at varying angles that correspond to the local dip after Shea et al., 1988 and Goodson, 2014.

Sample preparation required taking two sets of samples that were cut parallel and perpendicular to the foliation to investigate the major crystallographic axes that define the quartz strain ellipsoids suspended in the granitic matrix. From the twelve rock samples collected, two sets of thin section slides were developed, parallel and perpendicular to the foliation respectively, to analyze the deformation recorded in the microstructures of the granitic pluton. Circled number indicates samples measured at each location

Paramount in a meaningful discussion about the emplacement of the Tungstonia Granite is the geologic setting which frames the conversation in terms of larger geologic processes. The Mesozoic Sevier orogenic thrust belt left in its wake a north-northeast trending metamorphic belt of two-mica granitic intrusions and metamorphosed Paleozoic sedimentary rocks in the eastern Great Basin of western North America along the border between Nevada and Utah (Armstrong, 1968, Best et al, 1974). Mantle core complex metamorphism is widespread throughout the Mesozoic metamorphic belt, however the Kern Mountains and the Late Precambrian and Paleozoic carbonates that surround them appear to have deformed due to the forceful emplacement of the Tungstonia granite of and are surrounded by normal faults (Armstrong, 1968; Best et al., 1974, Barton & Trim, 1991, Sayeed et al., 1977). Stratigraphic studies and isotropic measurements of Rb-Sr and K-Ar values suggest that Tungstonia granite stopped ascent and emplaced 60 million years ago at an approximate depth of 10.5 km (Best et al., 1974; Ahlborn, 1977; Sayeed et al., 1977; Goodson, 2014). The normal faults surrounding the pluton seem to lack significant displacement to allow the passive emplacement of the ~51 sq. km Tungstonia Granite (Best et al., 1974; Goodson, 2014). Furthermore, significant strains and foliations observed allow the dismissal of tectonic accommodation as a reasonable means of transport and emplacement for the Tungstonia Granite. Homogenous nature of the Tungstonia granite as well as a lack of xenoliths and irregular boundary contacts seems to suggest a lack of stoping as a major emplacement mechanism (Armstrong, 1972; Sayeed, 1972; Best et al., 1974; Alhborn, 1977, Shea et al., 1988). The concordant contact dips uniformly at an approximate angle of 55^{o}, and border granites of the Tungstonia Granite are sheared with strong foliation that coincides with the foliations present in the surrounding dolostones; both of which are sub-parallel to the contact (Sayeed et al., 1977; Shea et al., 1988; Goodson, 2014). These foliations

fade with displacement away from the contact and are believed to have formed during the solid-state deformation associated with the buoyant rise that deformed the crystalline marginal granites and the surrounding dolostones, some of which exhibit lineation (Shea et al., 1988). Within the granite, deformed mica and quartz ribbons define foliation.

Period	Formation / Members		Thick-ness
QUAT	Alluvium, L. Bonneville seds.		0-200
MIO - PLIO	High-level alluvium		0-500
	Valley fill		0-2000 ?
OLIG	Intermediate lavas & tuffs		0-200
EOCENE	Skinner Canyon Granite		intrusion
CRET	Ibapah Granite		intrusion
PERMIAN	Tungstonia Granite		intrusion
	Park City Group	NULL	500
	Arcturus Fm		2000
PENN	Ely Limestone		1200
MISS	Chainman Shale		1100
	Joana Limestone		340
DEV	Pilot Shale		260
	Guilmette Formation		2300
	Simonson Dolomite		700
	Sevy Dolomite		800-1100
SILURIAN	Laketown Dolomite		800
ORD	Ely Spring Dolomite		250-400
	Eureka Quartzite		200-325
	Crystal Peak Dolomite		30-120
	Watson Ranch Qtzt		30-150
	Pogonip	Lehman Fm	180-300
		Kanosh Shale	300-500
		Lower Pogonip undivided	1800-2000
CAMB	Notch Peak Formation		310
	Corset Spring Sh		40
	Orr Formation		100-600
	Lamb Dolomite		1000
	Trippe Limestone		0-600
	Young Peak Dolomite		500
	Abercrombie Formation		2500
	Pioche Fm	Busby Qtzt Mbr	500
		Cabin Sh Mbr	500
	Prospect Mountain Quartzite		3300
pC (PROT)	G-phyllite, metasiltstone		300
	F- feldspathic quartzite		1200
	E-phyllite & quartzite		1500
	D-feldspathic qtzt		1100
	C-rnicaceous quartzite		1500
	B-pelitic schist		2000
	7-feldspathic qtzt		4500
	6-metasiltstone, micaceous quartzite, & pelitic schist		4000
	5-metadiamictite, cg, qtzt		1200
	4-micaceous quartzite		600
	3-metasiltstone, qtzt, cg		1000
	2-marble		160
	1-pelitic		140

Figure 7. Stratigcraphic section that illustrates the geologic background of the Kern Mountains. Geologic column was originally measured in Trout Creek (in western Utah, approximately 15 miles from where the Kern Mountains reside within the Mesozoic metamorphic belt) Thicknesses are given in feet. Modified from Hintze & Kowallis, 2009

CHAPTER II

METHODS

Samples were collected for study by optical microscopy and lattice preferred orientations (LPOs) of deformed quartz ‘ribbons’ believed to be recrystallized individual quartz grains. Previously composed maps from Best et al., (1974) and Ahlborn, (1977) were utilized as an initial base map for traverse selection and sample collection by Dr. Andreas Kronenberg and William Shea. Seven linear transverses were selected for study surrounding the concordant granite-carbonate contact. Traverse ‘E’ (which runs near the eastern edge the southern contact margin) from Shea et al., 1988 was selected for study due to the preservation of deformed quartz ‘ribbons’ foliation parallel to the contact that describe the history of solid-state deformation along the marginal granites, and due to the trend of decreasing strain observed in samples closer to the center of the pluton. Foliation poles were plotted in the granitic body and in the surrounding dolostones. Foliations trend sub-parallel to the contact between the pluton and surrounding country rock and indicates solid-state deformation as the chilled crystal margin was subject to stresses associated with diapiric rise and/or inflation. Previously collected samples were reoriented in lab with respect to their position relative to the granite-dolostone contact, and thin sections were cut perpendicular to the foliation which is coincident to the contact dipping at an assumed constant angle of 55^{o}.

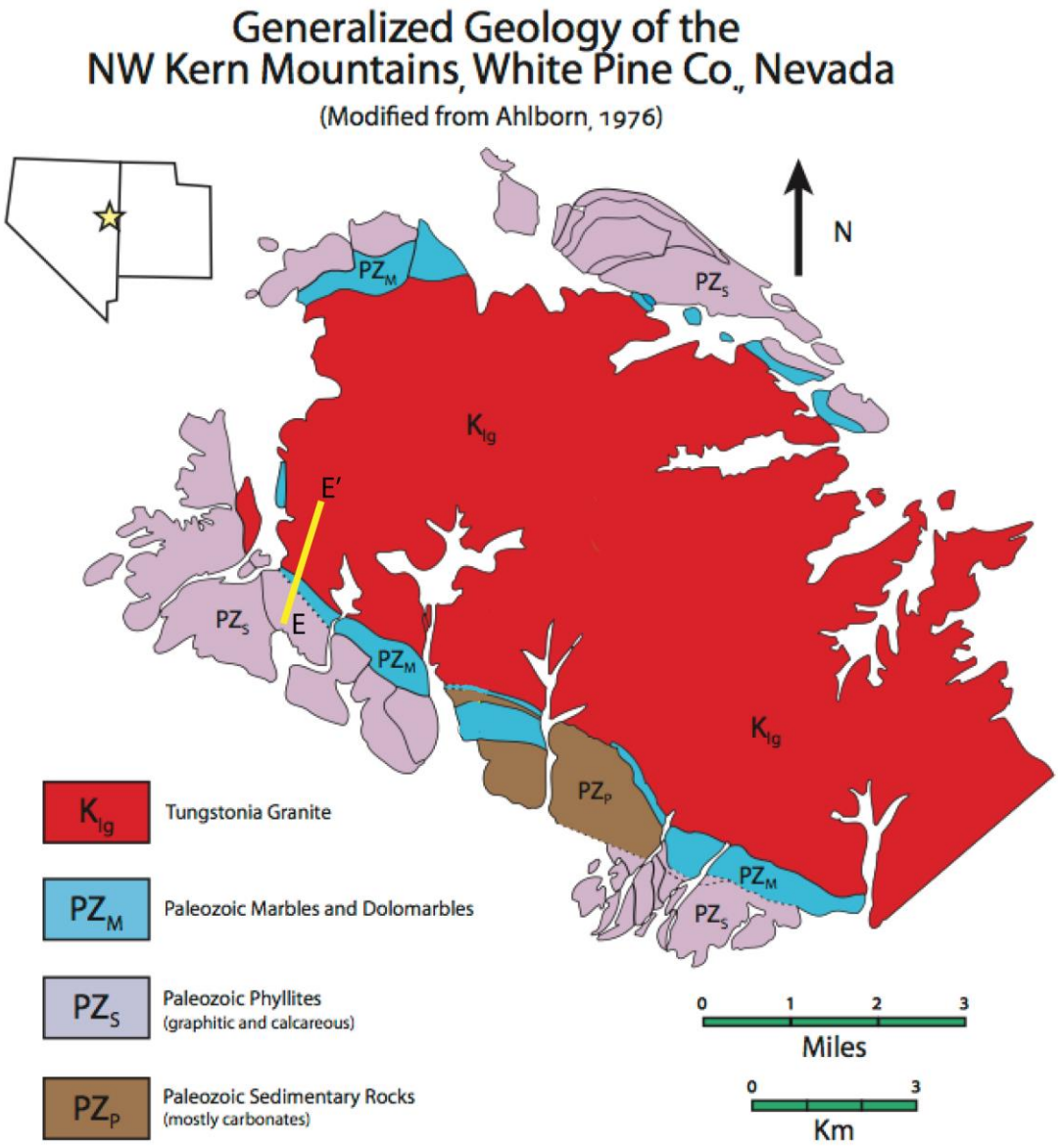

Figure 8. Generalized geologic field map of Tungstonia pluton, Kern Mountains after Shea et al., 1988, Goodson, 2014, and modified after Ahlborn, 1976. Yellow bar indicates traverse 'E' that was selected for investigation. Granite samples were collected ~1400 meters into the pluton body and orthogonal thin sections were developed perpendicular to the granite-dolostone contact

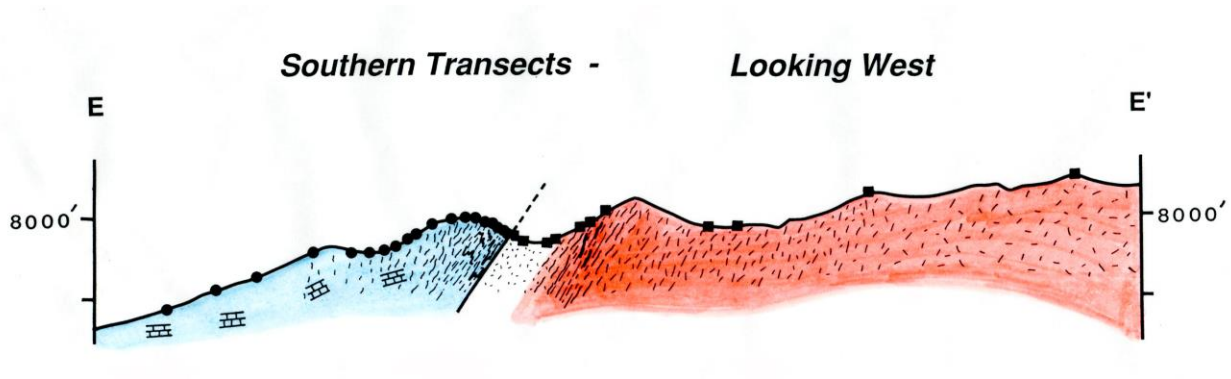

Figure 9. Cross section of Traverse E in the Tungstonia granite and the surrounding carbonates. Colors match above legend (i.e. red represents the Tungstonia granite and blue represents the Paleozoic Marbles and Dolomarbles)

The principle method of analysis has been optical microscopy of deformation microstructures due to solid-state deformation of quartz and mica in the marginal granites. These microstructures are believed to be recorded within the cooling, crystallized margin of the pluton as the freshly solid igneous rock is immediately subjected to high shear stresses along the margins and high compressive stresses in the direction of its ascent associated with intrusion. Quartz and micas appear to have been deformed by high strains, and their orientation defines the foliations. Feldspars, conversely, appear largely undeformed. Quartz ribbons that exhibit undulatory extinction are interpreted to be recrystallized individual quartz grains that act to record the strains present throughout the history of solid-state deformation driven by the buoyant forces that cause the crystallizing granite to ascend. Both feldspars and micas truncate quartz ribbons in some cases and can impede the growth of recrystallized quartz ‘ribbons’. Consequentially, Tungstonia granite quartz can only infer a percentage of the total accumulated strain due to intermediate and high finite strains being lost after quartz grain recrystallization.

Locally high aspect ratios recorded in deformed quartz “ribbons” near the contact aureole decrease with displacement away from the contact where the quartz grains are less deformed and more equigranular. Aspect ratios were recorded by measuring the major and minor axis to evaluate the distribution of strain. It is significant to note that the b-axis and c-axis measurements were normalized to a common c-axis measured in tandem with a. These distributions can be compared with viscous diaper models (Marsh, B., 1982; Schmeling, H. et al., 1988; Polyansky, O.P et al,. 2009). Flinn diagrams are used to describe the strain ellipsoid of the dynamic recrystallized quartz grains and describe the trend of distributed strains across the traverse. This is done by comparing ratios of finite strain axes (a/b) to (b/c).

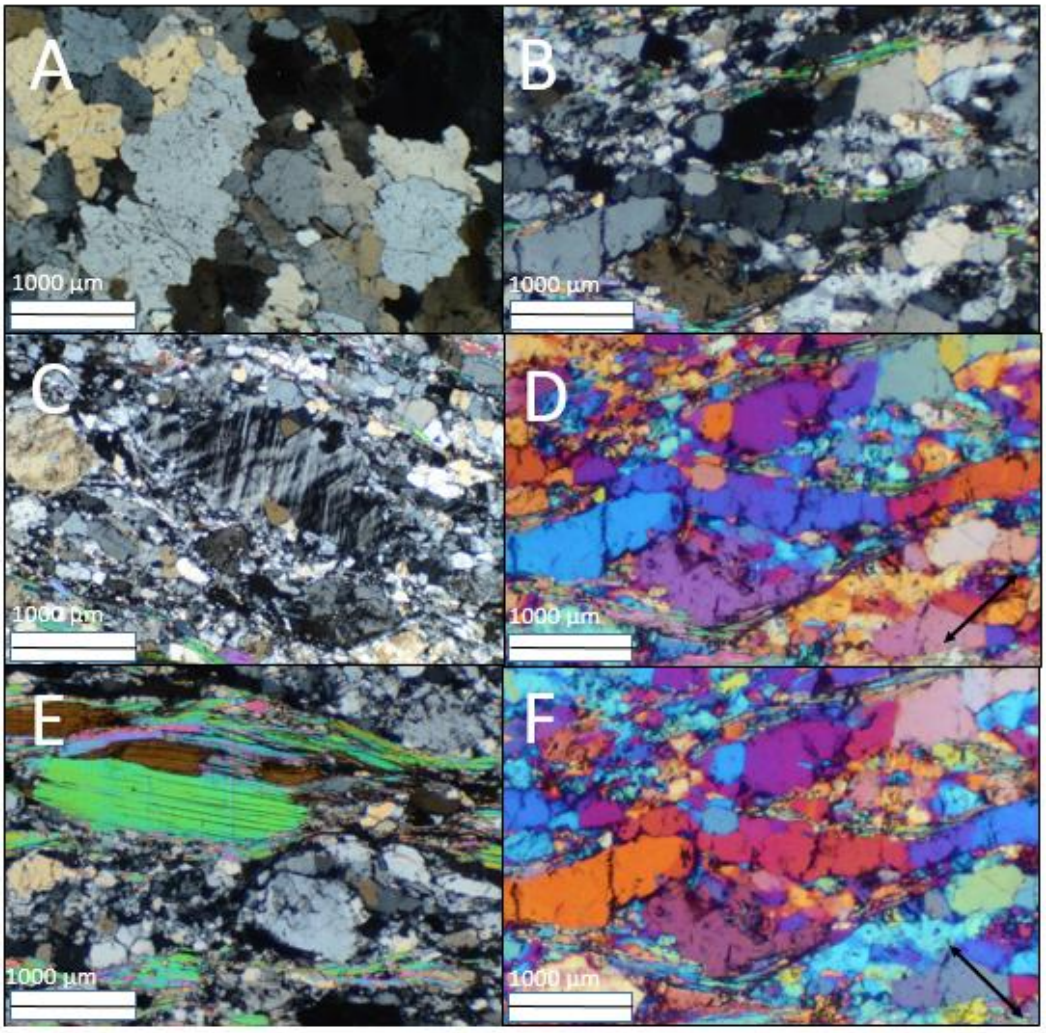

Figure 10. Preserved crystalline microstructures of the Tungstonia pluton. (A) Equigranular igneous texture quartz grains from the center of the pluton under cross polarized light. (B) Highly sheared marginal quartz grain under cross polarized light. (C) Mildly deformed microcline feldspar grain. (D) Same deformed quartz as D under cross polarized and gypsum plate light. Orientation of slow gypsum ray shown in image as the black arrow. (E) Aligned deformation 'fish' micas define foliation along with quartz. (F) Same deformed quartz under cross polarized and gypsum plate light. Orientation of slow gypsum ray shown in image as the black arrow. Scale given

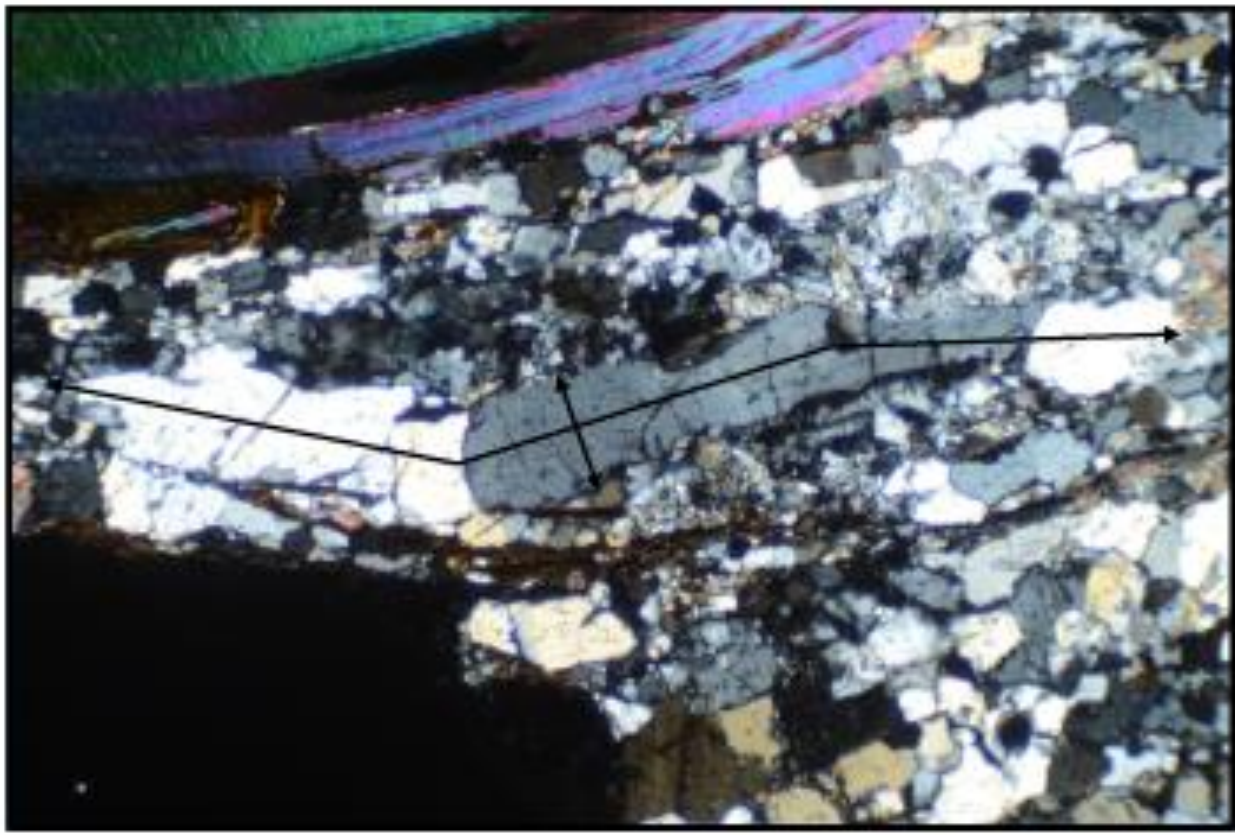

Figure 11. Illustration of microscopic measurements of quartz strain axes. Arrow indicate measurements of both the major and minor axis. The minor axis is measured at multiple approximately equidistant locations (not shown) along the grain to average together regional variations. Scale not shown

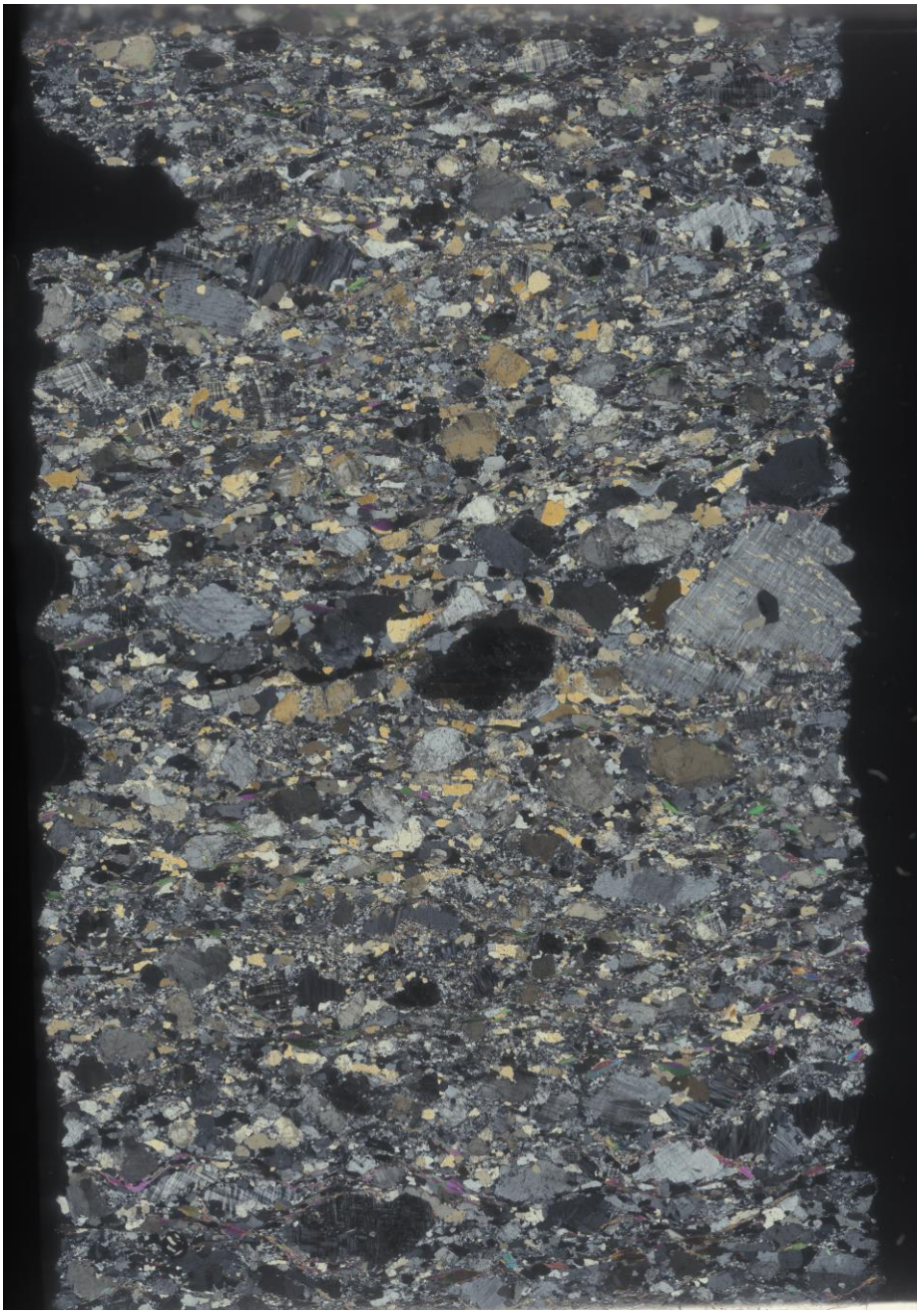

Figure 12. Full scan of thin section EG-2 that faces northwest and parallels observed lineations and represents the a- and c- finite strain axes. Section shown in plane polarized light. This section was selected for investigation of lattice preferred orientations (LPOs). Scale not shown

C-axis lattice preferred orientations align based on the type of deformation mechanism that reflects the strain. C-axis measurements can be done optically as the interference figure indicates the orientations of the c-axis for uniaxial minerals where the horizontal and vertical isogyres cross. When plotted on an equal area stereonet, the distribution pattern of lattice preffered orientations can indicate intragranular crystallization deformation mechanisms as well as indicate a sense of symmetrical or asymmetrical shear. These models can then be compared to other studies to understand the mechanisms that generated the crystalline fabric (Tullis et al., 1973, Lister and Hobbs, 1980, Dawson and Wenk, 1999). 300 individual measurements where made manually using a universal stage microscope and plotted in Allmendinger's Stereonet 9. Contours are generated by Kamb's contouring method (Kamb, 1959)

Figure 13. Universal Stage Microscope used to measure lattice preferred orientations of sample EG-2 that shows major axis a and minor axis c

CHAPTER III

RESULTS

Solid-state deformation microstructures of quartz ellipsoids and their dimensions reflect strain and emplacement conditions at the Tungstonia granite's last buoyant motion before emplacement in the surrounding dolostone country rock. Finite strain ellipsoid axes have been denoted a, b ,c with a being the axis of major strain, b being the axis of intermediate strain, and c being the axis of minor strain. Measurements have been collected from orthogonal thin sections cut perpendicular the foliation preserved in traverse E, and the ellipsoid major axis dimensions have been normalized to share a common minimum c-axis measurement.

Table 1. Table of ellipsoid grain measurements from Kern Mountain Tungstonia granite. Axis measurements used to determine strain ellipsoid and analyze the change in strain with respect to the granite-dolostone contact. *denotes that these measurements were normalized to a common c-axis. Generation of a Flinn diagram was made possible by these measurements

Sample	Distance From Contact (m)	Mean a-axis (µm)	Mean b-axis* (µm)	Mean c-axis* (µm)	Mean Grain Shape (a/c)	Mean Grain Shape (b/c)	Total # of grains measured
EG-2	7.7	2585.7	1651.4	227	11.4	7.3	30
EG-3	38.7	1842	1368	132.7	13.9	10.3	29
EG-5	108.5	1674.5	1446.2	176.4	9.5	8.2	23
EG-6	116.1	2637	2244.6	361	7.3	6.2	27
EG-7	154.7	2859	2993.5	572.75	5.0	5.2	21
EG-8	170.2	1200.0	914.1	127.7	9.4	7.2	41
EG-9	201.1	2979.6	3354.3	521.0	5.7	6.4	29
EG-10	487.4	1992.0	1234.5	252.2	7.9	4.9	34
EG-11	557.1	1450.8	1692.9	768.2	1.9	2.2	41
EG-13	835.6	1625.0	1332.8	272.2	5.9	4.9	40
EG-14	1330.8	1388.0	1404.5	758.0	1.8	1.8	30

Aspect ratios of quartz clusters near the granite-dolostone contact are exceedingly high and follow a decreasing trend toward more equant grains away from the contact suggesting that high intrusive stresses acted on this cooling magma body, and that stresses receded as the buoyant granite lost its heat and energy to the surroundings during emplacement of the Kern Mountain pluton. Consequently, the solid-state quartz deformation only records the last buoyant motion of the pluton before it completely crystallizes and emplaces. These high aspect ratios, particularly at and near the point of contact, suggest forceful emplacement as a mechanisms for pluton intrusion. Grain axis measurements were then plotted on a structural Flinn diagram to better describe the strain ellipsoid and to generate a 3D view of our measured grains. Measurements seem to predominantly fall in the compressional, pure shear, K=0 strain ellipsoid zone. The strong correlation and position of these measurements isn't intuitive to the expected simple shear expected close to the granite-dolostone contact but will be interpreted in the discussion section.

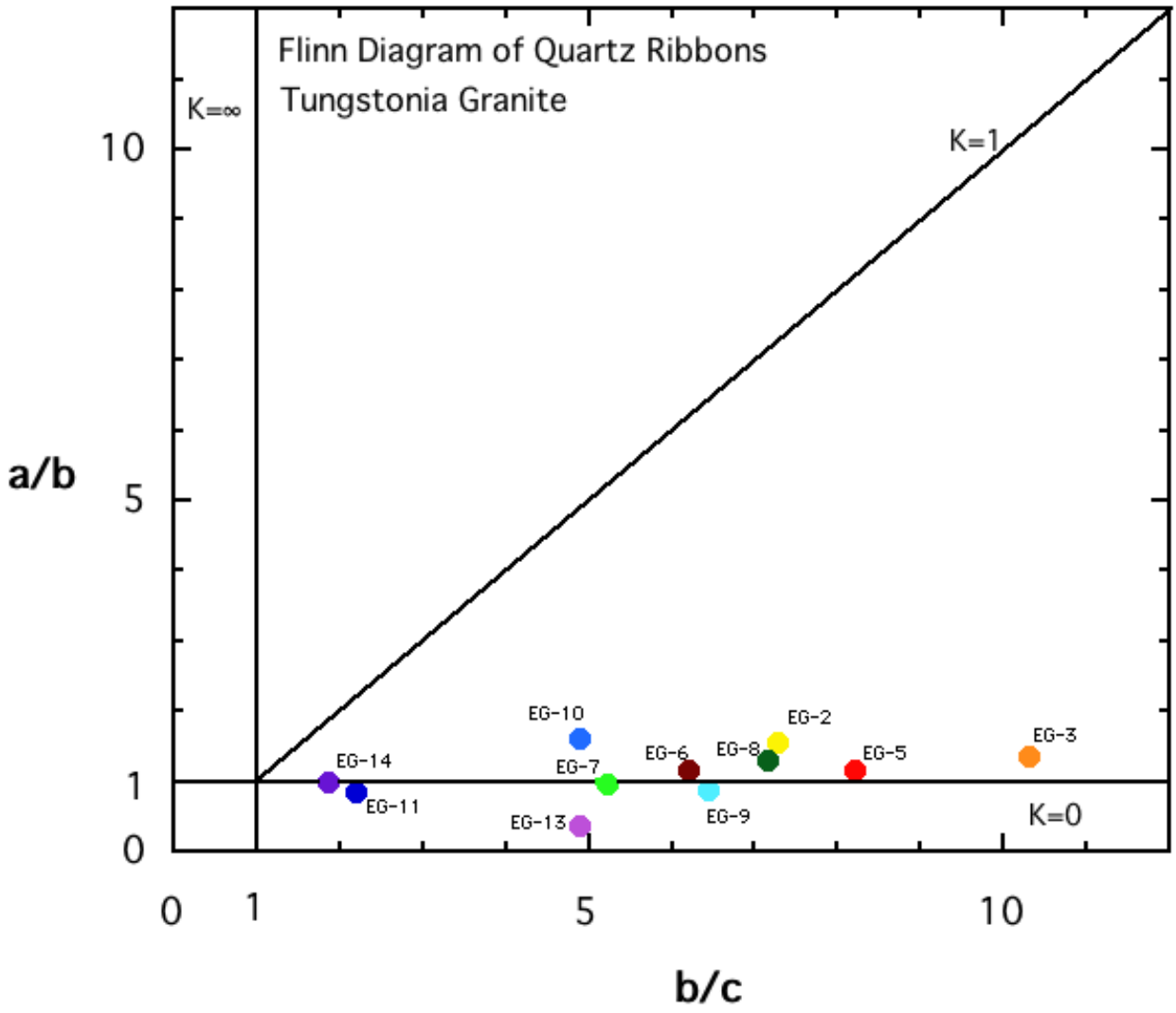

Figure 14. Flinn diagram of Tungstonia granite quartz ribbons. a/b vs b/c graph to represent the 3D strain ellipsoid of quartz grains with locations within traverse denoted next to the respective data points. Measurements typically fall between the pure shear and simple shear zones with a trend and inclination towards the pure shear zone.

Crystallographic lattice preferred orientations are plotted using Stereonet 9 and Kamb contours as well as actual data points are plotted below. A contour interval of 2 is used with a max contour of 4. C-axis lattice preferred orientation distributions appear to be an asymmetrical variation of diffused cross-girdle pattern typical of basal and prism slip and simple shear.

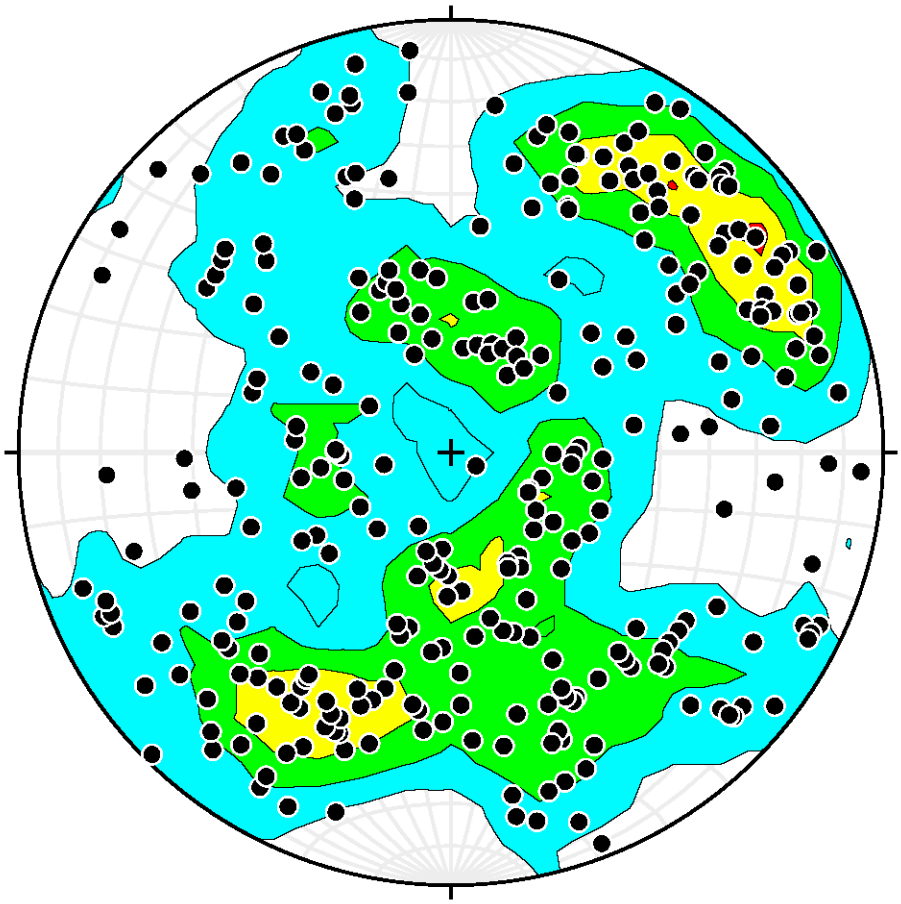

Figure 15. Lower hemisphere of an equal area stereonet with Kamb contours plot of lattice preferred orientations of the Tunstonia granite's deformed quartz ribbons measured in thin section EG-2, parallel to lineation, is shown above. Sample is ~7.7 meters away from the granite-dolostone contact. 300 lattice preferred orientations measured and shown. Polychromatic color gradient shows areas of low LPO density as blue to those of high LPO density as red

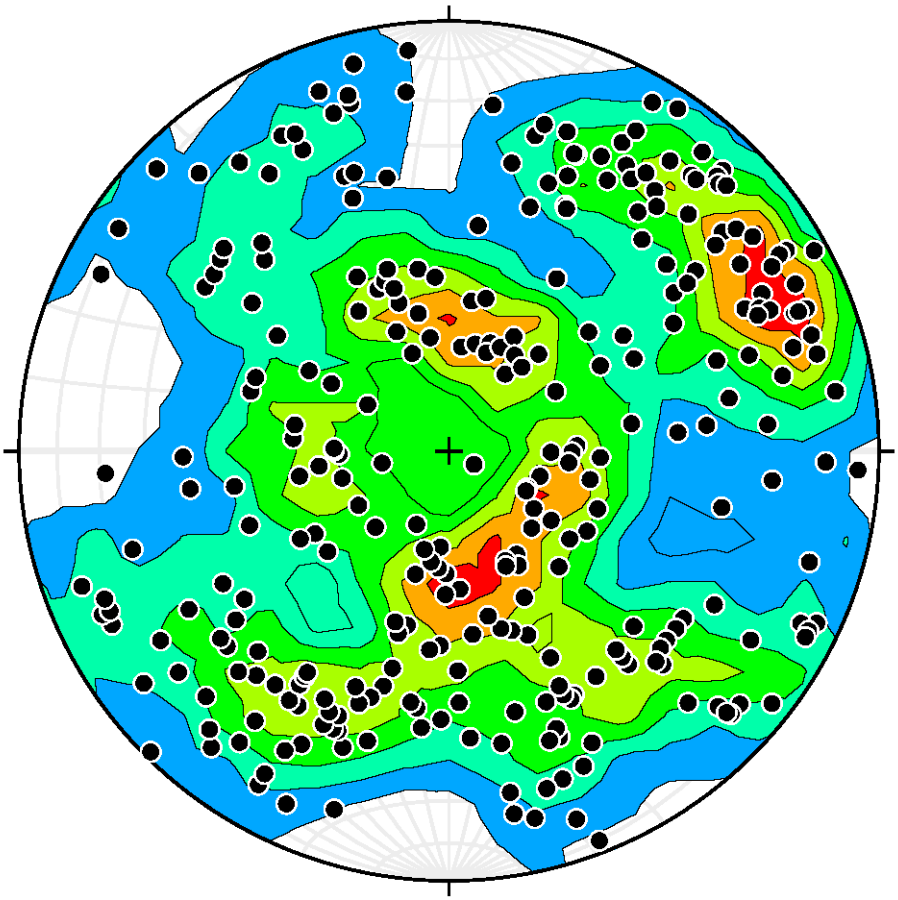

Figure 16. Same plotted c-axis lattice preferred orientations as above with an applied Terzaghi correction of trend 9 and a maximum correlation factor of 2. Given to better illustrate density concentrations and express a distribution pattern. Polychromatic color gradient shows areas of low LPO density as blue to those of high LPO density as red

CHAPTER IV

DISCUSSION

"The form of an object is a diagram of forces"

-D'Arcy Wentworth Thompson

Field observations and measurements initially collected by William Shea and Andreas Kronenberg (et al. 1988) provided the fundamental observations necessary to begin this study of the forceful emplacement of the Tungstonia granite. Poles of foliations that paralleled the contact were mapped. Lineations, rolled augens, and other mesoscopic and microscopic evidence of asymmetrical shear began to infer forceful emplacement by diapiric ascent that coincided with previous studies and observations (Armstrong, 1968; Best et al., 1974; Barton & Trim, 1991; Ahlborn, 1977; Sayeed et al., 1977, Shea et al., 1988). Study of the surrounding carbonates by Kyle Goodson (2014) developed an understanding of the strain rate-temperature relationship that allowed non-linear, laminar flow of dolostones by thermal weakening. Penetrative strains associated with the intrusion and emplacement of the Tungstonia granite left dolostone strain ellipsoids and lattice preferred orientations that suggest asymmetrical, simple shear, dislocation creep deformation recorded in the carbonates close to the granite-dolostone contact (Delle Piane et al., 2008; Goodson, 2014). Optical microscopic of grain shape and c-axis lattice preferred orientations analysis of quartz samples within the Tungstonia granite aims to further the understanding of this forceful emplacement event.

Strain ellipsoids from quartz ribbons in the Tungstonia granite seem to indicate a prevailing compressional strain that is typically associated with models of inflation and laccolith intrusion (Clifford, 1972; Holder, 1979). However, this is challenges the strain ellipsoids preserved in the surrounding carbonate rocks and the lattice preferred orientations observed in both the carbonates and the Tungstonia granite itself (Goodson, 2014). The crystalline granite and the microscopic fabrics recorded there in represent the final snapshot of a complex, moving curiosity. In order to better explain these findings, Kyle Goodson's Flinn diagram of strain ellipsoids and Schmeling's models for granitic diapiric ascent (et al., 1988) and associated internally and externally strain are considered.

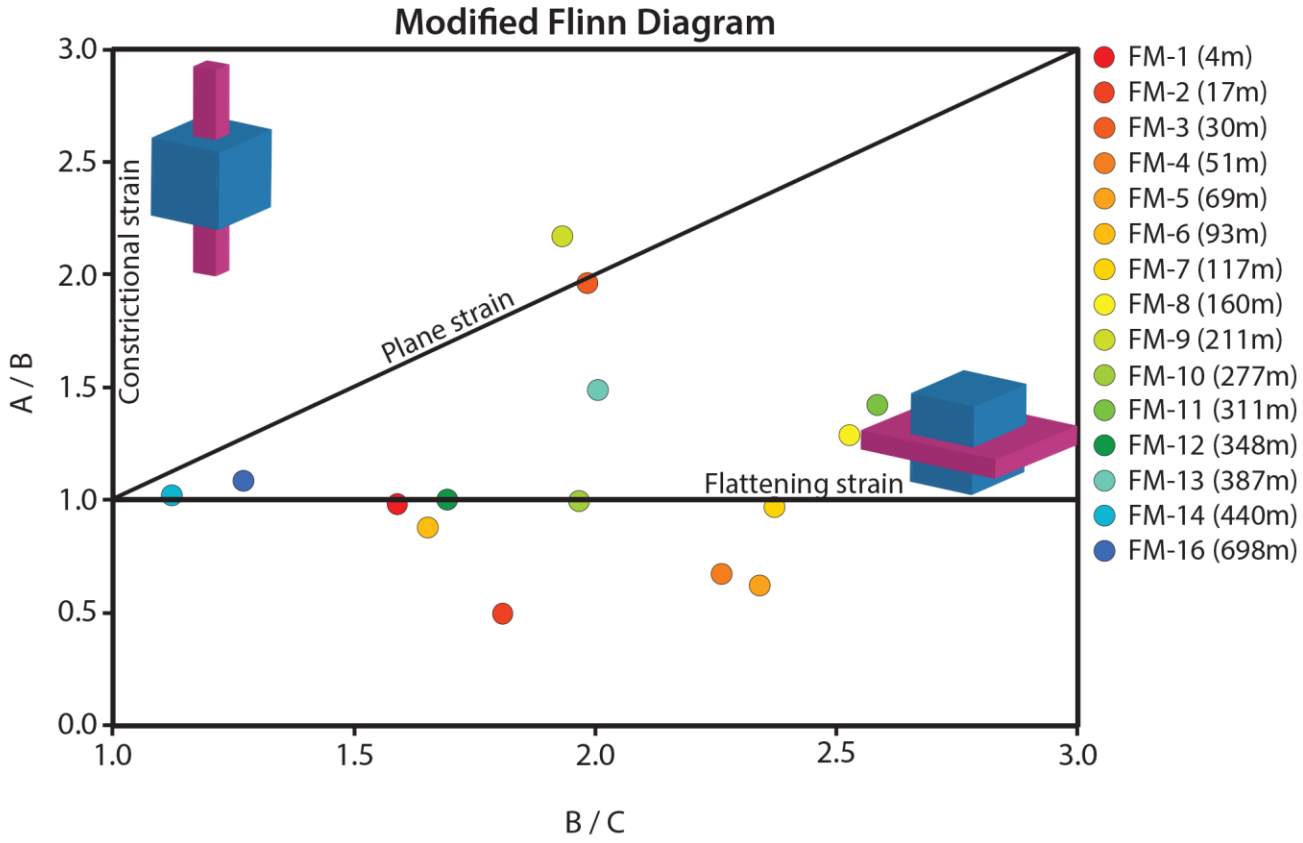

Figure 17. Modified Flinn diagram representing the strain ellipsoids present in the dolostones surrounding the Tungstonia granite after Goodson, 2014. Typical compressional strain extending to plane strain ellipsoids are represented in the carbonate samples. These samples were collected from the F traverse of the Tungstonia granite to the east of the E traverse. This traverse was selected due to lack of discontinuities, evidence of shear, and decreasing strain with relative to displacement from the contact (Goodson, 2014)

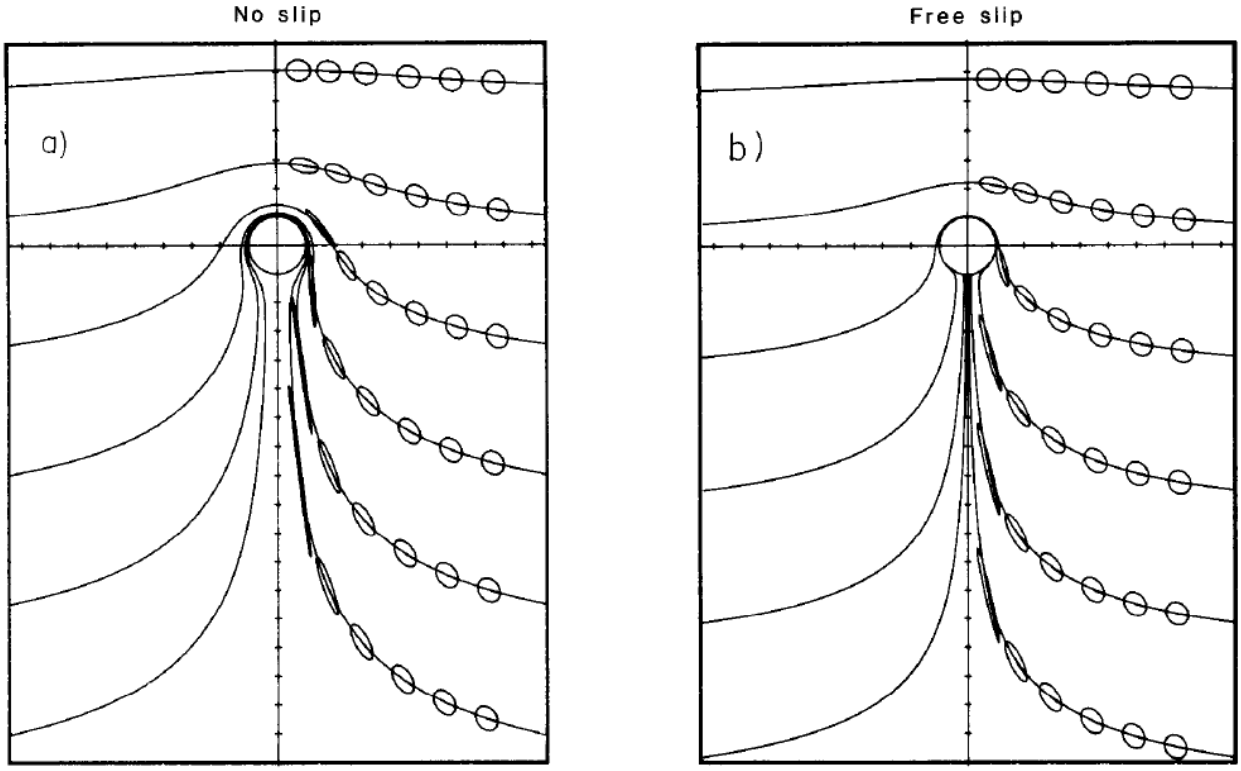

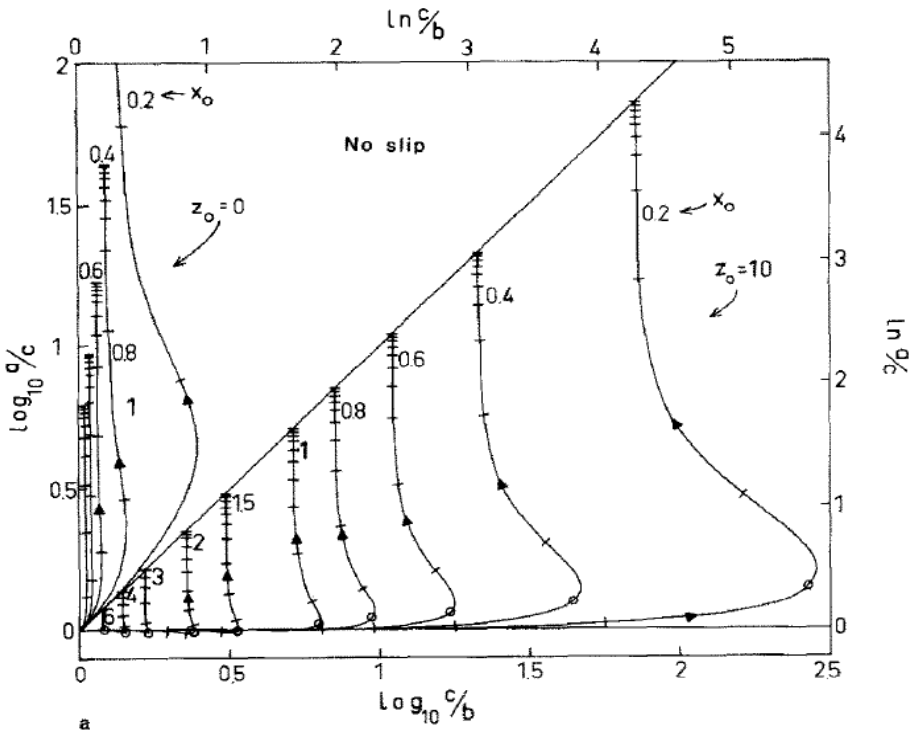
ln c/b
No slip
0.2 ← x_o
z_o = 0
z_o = 10
log_10 q/c
ln q/c
log_10 c/b
a

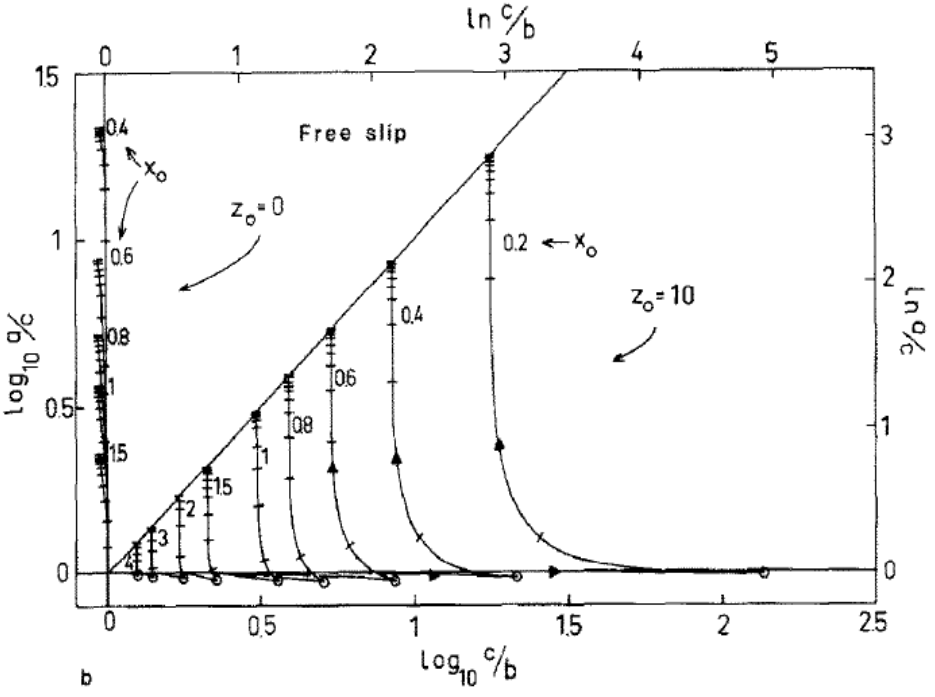
ln c/b
Free slip
x_o
z_o = 0
z_o = 10
log_10 q/c
ln q/c
log_10 c/b
b

Figure 18A, B, and C. Images after Schmeling et al., 1988 no slip and free slip, where no slip represents a model where fluid velocity on walls equals zero and where free slip represents a region of zero friction between the fluid and the wall, diapiric rise models in surrounding country rocks and their associated, modified Flinn diagrams. Rounded shapes plotted along lines surrounding the modeled sphere represent strain ellipsoids. Within the Flinn diagrams, “arrows indicate the time evolution of the strain ellipsoids as they move along the streamlines” (Schmeling et al., 1988). Extensional strain is plotted on the y-axis. Compressional strain is plotted on the x-axis. Plane strain is plotted on the slope starting at the origin.

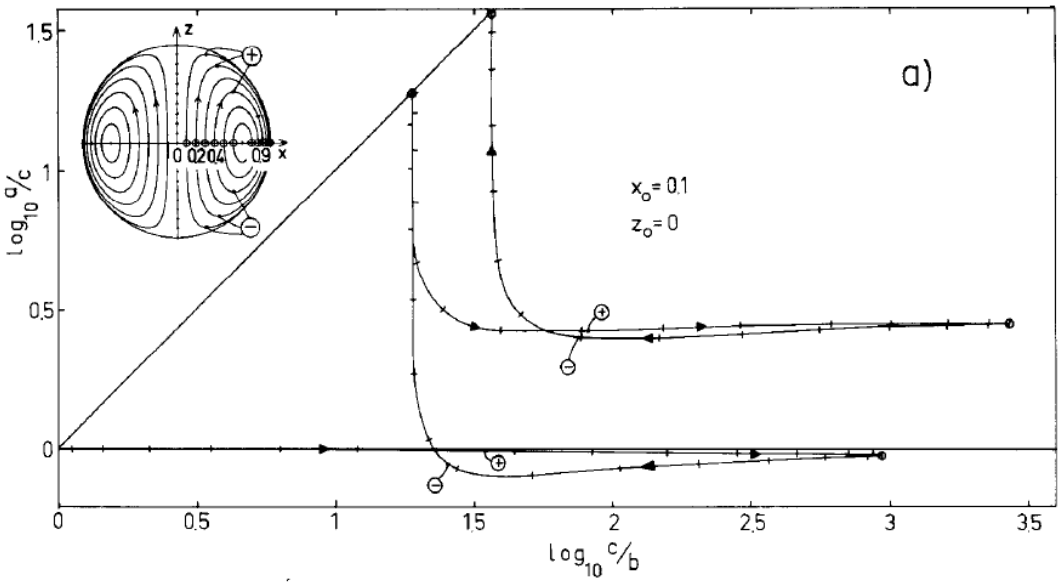

Figure 21. Diapiric model with associated Flinn diagram representative of strain ellipsoids generated within the rising diapir after Schmeling et al., 1988

Contrasting data from the Flinn diagrams that represents the Tungstonia granite and the carbonates that surround it can be compared to Schemling's models for diapiric ascent. The progression of strain ellipsoids initially travels along the pure shear, compressional strain region before evolving to ellipsoids of simple shear and plane strain. The model seems to suggest a long history of pure shear is expected before an eventual exponential trend toward simple shear is recorded in both the ascending diapir and in the thin, soft veil of country rock that surrounds it (Schmeling et al., 1988). The Paleozoic carbonates surrounding the Tungstonia granite are inferred to better record plane strain than the rising pluton itself due to thermal softening and temperature dependent viscosity are of importance in diapir ascent (Schmeling et al., 1988; Vilgneresse & Clemens, 2000). Strain ellipsoid analysis within the Tungstonia granite appears to record a longer history of injection and ascent wherein crystallographic axes dimensions reflect the compressional strain relics from their contact with the diapir-country rock contact. The lattice preffered orientations record a more recent history and reflect the grains travel through simple shear margins. The nature of lattice preferred orientations to adapt to echo their changing environments is documented in the convection of mantle derived olivine (Dawson & Wenk, 2000). Thus, a more thorough investigation of lattice preferred orientation adaption to convection stress fields in quartz is important to fully understand forceful emplacement.

CHAPTER V

CONCLUSION

Optical microscopic analysis of strain ellipsoids dimensions and c-axis lattice preferred orientations of quartz grains within the Tungstonia granite of eastern Nevada provides insight into conditions present at the final ascending act of this 51 sq. km giant. A history of compressional strain that evolves to plane strain coincides with the internal granitic flow up and then down across its margins. Strain ellipsoids from recrystallized quartz ribbons seem to better record the Tungstonia granite's prolonged ascent and compression while lattice preferred orientations seem to echo the later simple shearing events or the transformation from compressional to plane strain. Regardless, forceful emplacement by means of diapiric ascent and/or inflation prevails as the most reasonable model for the transport and emplacement of the Tungstonia granite. Future work is intended and already being prepared for. Further lattice preferred orientation work is intended for other samples and in quartz grains that don't form sheared ribbons. Investigation into ancient stresses via paleopiezometric measurements of recrystallized grain sizes will give us significant insight into the Tungstonia granite's flow stress history.

REFERENCES

Ahlborn, R. C., 1977. Mesozoic-Cenozoic structural development of the Kern Mountains, eastern Nevada-western Utah. Brigham Young University Research Studies, Geology Series 24, Part 2, 117-131.

Armstrong, R.L., 1968. Sevier orogenic belt in Nevada and Utah. Geological Society of America Bulletin 79, no. 4, 429-458.

Barton, M. D., Trim, H. E., 1991. Late Cretaceous two-mica granites and lithophile-element mineralization in the Great Basin. In: Schafer, R. W., Wilkinson, W. H. (Eds.), Geology and Ore Deposits of the Great Basin, Geological Society of Nevada Symposium Proceedings, Geological Society of Nevada, 529-538.

Best, M., Armstrong, R., Graustein, W., Embree, G., Ahlborn, R., 1974. Mica granites of the Kern Mountains pluton, eastern White Pine County, Nevada, remobilized basement of the Cordilleran miogeosyncline. Geological Society of America Bulletin 85, no. 8, 1277-1286.

Bowen, N.L., 1948. The granite problem and the method of multiple prejudices. In: Gilily, J., et al. (Eds.). Origin of Granite, 28. Geological Society America Memoirs, pp. 22-90.

Clemen, J.D, 1998. Ovservations on the origins and ascent mechanisms of granitic magmas. Journal of the Geological Society, London 155, 843-851.

Clifford, P.M., 1972. Behavior of an Archean granitic batholith. Canadian Journal of Earth Sciences 9, 71-77.

Daly, R.A., 1903. The mechanics of igneous intrusion. American Journal of Science 16, 4th ser., 107-126.

Dawson, P. R.,Wenk, H. R., 2000. Texturing of the upper mantle during convection. Philisophical Magazine A, Vol. 80, No. 3, 573-598

Delle Piane, C.D., Burlini, L., Kunze, K., Brack, P., Burg, J.P., 2008. Rheology of dolomite: large strain torsion experiments and natural examples. Journal of Structural Geology 30, 767-776.

Gerbi, C., Johnson, S.E., Paterson, S.R., 2004. Implications of rapid, dike-fed pluton growth for host-rock strain rates and emplacement mechanisms. Journal of Structural Geology 26, 583-594.

Gilbert, G.K., 1877. Report on the geology of the Henry Mountains. U.S. Geographical and Geological Survey of the Rocky Mountain Region, 160 p.

Goodson, K.P., 2014. Penatrative Deformation of Dolostones During Contact Metamorphism and the Forceful Emplacement of the Tungstonia Granite, Kern Mountains, Nevada, M.S. Thesis, Texas A&M University, 1-80 pp.

Hintze, L.F., Kowallis, B.J., 2009. Geologic history of Utah: a field guide to Utah's rocks. Brigham Young University Geology Studies, Special Publications 9, 225 p.

Hunt, C.B., Averitt, P., Miller, R.L., 1953. Geology and geography of the Henry Mountains region, Utah. U.S. Geological Survey Professional Paper 228, 234 p.

Holder, M.T., 1979. An emplacement mechanism for post-tectonic granites and its implications for their geochemical features. In: Atherton, P.P., Tarney, J. (Eds.), Origin of granite batholiths; geochemical evidence: Orphington, England, Shiva, 148 p.

Kamb, W.B., 1959. Ice petrofabric observations from Blue Glacier, Washington, in relation to theory and experiment. Journal of Geophysical Research 64, no. 11, 1891-1909.

Lister, G. S., Hobbs, B.E., 1980. The simulations of faric development during plastic

Marsh, B., 1982. On the mechanics of igneous diapirism, stoping, and zone melting. American Journal of Science 282, 808-855.

Miller, R.B., Paterson, S.R., 1999. In defense of magmatic diapirs. Journal of Structural Geology 21, 1161-1173.

Morgan, S.S., Law, R.D., Nyman, M.W., 1998. Laccolith-like emplacement model for the Papoose Flat pluton based on porphyroblast-matrix analysis. Geological Society of America Bulletin 110, 96-110.

Pollard, D.D., Johnson, A.M., 1973. Mechanics of growth of some laccolithic intrusions in the Henry Mountains, Utah, Part 2. Tectonophysics 18, 311-354.

Polyansky, O.P., Korobeynikov, S.N., Babichev, A.V., Reverdatto, V.V., Sverdlova, V.G., 2009. Computer Modeling of Granite Magma Diapirism in the Earth's Crust. Doklady Earth Sciences 429, no. 8, 1380-1384.

Polyansky, O.P., Babichev, A. V., Korobeyniko, S. N., Reverdatto, V. V., 2010. Computer modeling of granite gneiss diapirism in the earth's crust: controlling factors, duration, and temperature regime. Petrologiya 18, 450-466.

Sayeed, U.A., 1972. A note on the Kern Mountains plutonic complex, White Pine County, Nevada, and Juab County, Utah. Geological Society of America: Abstracts with Programs 4, no. 6, 407.

Sayeed, U.A., Treves, S.B., Nelson, R.B., 1977. Geochemistry and hydrothermal alteration of the Kern Mountains plutonic complex, White Pine County, Nevada and Juab County, Utah. Geologische Rundschau 66, no. 1, 614-644.

Shaw, H. R., 1980, Fracture mechanisms of magma transport from the mantle to the surface, *in* Hargraves, R. B. ed., Physics of magmatic processes: Princeton, N.J., Princeton Univ. Press, p. 201-264.

Shea, W.T., Kronenberg, A.K., Erksine, B., 1988. Diapiric emplacement of granitic magma: a natural example. Geological Society of America: Abstracts with Programs 20, A272.

Schmeling, H., Cruden, A., Marquart, G., 1988. Finite deformation in and around a fluid sphere moving though a viscous medium: implications for diapiric ascent. Tectonophysics 149, 17-34.

Tikoff, B. de Saint Blanquat, M., Teyssier, C., 1999. Translation and the resolution of the pluton space problem. Journal of Structural Geology 21, 1109-1117.

Tikoff, B., Teyssier, C., 1992. Crustal-scale, en echelon 'P-shear' tensional bridges: A possible solution to the batholothic room problem. Geology 20, 927-930.

Tullis, J., Christie, J. M., Griggs, D. T., 1973. Microstructures and preferred orientations of experimentally deformed quartzites. Geological Society of America Bulletin, v. 84, p. 297-314

Vilgneresse, J. L., Clemens, J. D., 2000. Granitic magma ascent and emplacement: neither diapirism nor neutral buoyancy. Geological Society, London, Special Publications v. 174, p. 1-19.

Weinberg, R., Podladchikov, Y., 1995. The rise of solid-state diapirs. Journal of Structural Geology 17, 1183-1195.

Zak, J., Paterson, S.R., 2006. Roof and walls of the Red Mountain Creek pluton, eastern Sierra Nevadas, California (USA): implications for process zones during pluton emplacement. Journal of Structural Geology 28, 575-587.